



Utilizing Reduced Graphene Oxide-Iron Nanoparticles Composite to Enhance and Accelerate the Removal of Methyl Blue Organic Dye in Wastewater

Tilak Narayan Ghosh^{a*}, Sitangshu Sekhar Pradhan^b, Mainak Ray^c, Barun Mondal^d, Subinoy Jana^d, Pallabi Paul^c,
Salil Kumar Sarkar^b & Subhas Chandra Saha^f

^aDepartment of Electronics, Midnapore College (Autonomous), Midnapore 721 101, India

^bDepartment of Physics, Midnapore College (Autonomous), Midnapore 721 101, India

^cR&D and Innovation, HPCL-Mittal Energy Ltd, Bhatinda (Punjab) 151 301, India

^dDepartment of Chemistry, Midnapore College (Autonomous), Midnapore 721 101, India

^eDepartment of Chemistry, IIT Guwahati, Assam 781 039, India

^fDepartment of Electronics, Vidyasagar University, Midnapore 721 102, India

Received 8 August 2022; accepted 20 October 2022

In this work, a nano-composite is used to remove dye from wastewater of different industries. For this purpose, the synthesis of a magnetic 1:1 composite made of iron nanoparticles (NPs) using reduced graphene oxide is a novel technique and tested for Methyl Blue (MB) dye adsorption from aqueous solution. In this study Fe nanoparticles in reduced Graphene composite (FGOC) has been prepared using Graphene Oxide (GO). X-ray diffraction, FTIR spectroscopy and Raman spectroscopy, are used to identify the structures. Many methods have been developed for MB removal in wastewater. One of the most popular methods is adsorption because it is simple and high-efficiency, and the adsorbent is crucial. It reached a maximum MB adsorption at pH 7. The kinetic study indicated that the adsorption of MB process was fitted well to the quasi-first-order and quasi-second-order kinetic models. The isotherm study revealed that the MB adsorption process obeyed the Langmuir and Freundlich adsorption Isotherms models. The GO adding content and absorption conditions on the methyl blue removal efficiencies were investigated. This adsorbent is easily recovered by an external magnetic field from the treated wastewater and has high reusability.

Keyword: Nanoparticle; Graphene oxide; Dye removal; Kinetics of adsorption; Adsorption isotherm

1 Introduction

Leather, textiles, paper, and cosmetics are among the many industries that use dyes. The coloured wastewater from similar industries create severe environmental pollution. For environmental and health reasons, before wastewater is discharged, it is important that organic dyes are to be removed. The presence of coloured dyes in wastewaters of industries is hazardous to the ecology and human health. Many research works have been reported on this subject. For dyes graphene based nanomaterials, mainly Graphene Oxide (GO) and also reduced Graphene Oxide (rGO) are effective adsorbents of the dyes in wastewaters¹⁻⁸. So, it is expected that a properly synthesized composite of iron nanomaterials and GO/rGO will be efficient adsorbents for dye removal and cost of dye removal will be reduced. As the composite is magnetic it can be simply detached from the solution

with an outside magnet after the adsorption process completed. Graphene Oxide (GO) carries negative surface electrostatic due to the presence of oxygen-containing groups, which is helpful to its adsorption of organic dyes and metal ions in the aqueous phase. Due to its delocalized π -electron system and large surface area ($\sim 2600 \text{ m}^2 \text{ g}^{-1}$), graphene is a promising adsorbent candidate^{9,10}. But, the recovery of pure GO from treated wastewater is difficult due to its excellent hydrophilicity and size. Based on those problems, integrating GO with other materials becomes the popular method for its modification. The combination of GO with magnetic Fe_3O_4 could provide the composite with good hydrophilicity and recyclability. Standard preparation methods of magnetic nano-adsorbents include the co-precipitation method, hydrothermal method, oxidation (reduction) precipitation method, high-temperature oxidation method¹¹⁻¹². The GO/ Fe_3O_4 nanocomposites have recently been investigated by Jaleh *et al.*¹³, which showed high catalytic activity for reducing methylene

*Corresponding authors:
(Email: tilak.narayan.ghosh@midnaporecollege.ac.in)

blue. This activity can be recycled and reused several times because of the magnetic separability. In a recent study by Ranjith *et al.*¹⁴, TiO₂-Co₃O₄ decorated graphene oxide nanocomposite has been shown to be useful in the removal of industrial pollution. Huong *et al.* had researched the preparation of GO-Fe₃O₄-Ag ternary nanocomposite by a one-pot hydrothermal treatment, whose saturated magnetization value was about 57.3 emu/g¹⁵. It can be a promising material for environmental catalysts. Liu *et al.* fabricated Fe₃O₄-GO through a hydrothermal method¹⁶. Jinendra *et al.* studied the preparation of Fe₃O₄@CFR@GO by hydrothermal method, which was proven to be very efficient in the adsorptive degradation of Evans blue dye¹⁷. Guo *et al.*¹⁸ studied Fe nanoparticles@graphene composite for dye removal. Pradhan *et al.*¹⁹ had synthesized Iron Oxide @ rGO composite for effective anionic dyes and Arsenic (V) elimination from water. The study of Fe₃O₄ embedded GO composite had been reported by Zhou *et al.*²⁰. Huong *et al.*²¹ had applied GO-Fe₃O₄ composite for dye removal. The degradation of dyes, by Fe⁰/Fe₃O₄⁰/graphene composite, had been studied by Choug *et al.*²². Nagi *et al.*²³ had studied dye removal by GO-Fe₃O₄ and GO-Fe₃O₄@ZrO₂.

In this paper, the main novelty is the development of reduced graphene oxide nanosheets with Iron Oxide that will be used as an eco-friendly adsorbent for toxic Methyl Blue dye in water treatment. We developed an adsorbent using a chemistry-based approach which is simple, low cost, and exhibits superior separation capability with an external magnet. We studied the detailed adsorption dynamics, isotherms, and kinetics of Methyl Blue dye. We used both first-order and second-order kinetic models to predict dye adsorption onto the nanocomposite surface together. To understand the Methyl Blue adsorption mechanism, we fitted the adsorption isotherm with both the Langmuir and Freundlich models. As discussed above, we have synthesized a composite of iron nanoparticles and rGO in rGO:Fe=1:1 ratio, following same procedure of Guo *et al.*¹⁸ & Pradhan *et al.*¹⁹. The XRD, FTIR, and Raman Spectra of the composites have been obtained. Then we have studied the dye (Table 1) removal by UV-Vis Spectrophotometer.

2 Experimental

2.1 Materials

Graphite powder (325 mesh) (Alfa Aesar), FeCl₃, NaBH₄, Methyl Blue (C I No. 42780) procured from

E. Merck, Ltd, (Mumbai, India) and deionized (DI) water were used for all the experiments.

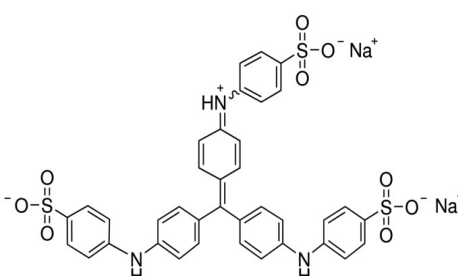
2.2 Methods

In a modified Hummers and Offeman method²⁴, graphine oxide (GO) was synthesized from graphite. For preparation of FGOC we used same procedure as our previous work¹⁹ and the steps of preparation of GO are described in details in one of our previous work²⁵. We used DI water to exfoliate graphite oxide. By repeated use of ultrasonication and ultra-centrifuging (to remove unexfoliated graphite oxide), we were able to produce a stable graphene oxide solution. To make a FGOC with Fe/GO mass ratio of 1:1, the required amount of FeCl₃ aqueous solution was mixed with GO dispersion. In order for the ion exchange reaction to be completed, the mixture was stirred for 12 hours. In the next step, an aqueous NaBH₄ solution, prepared in fresh was stirred into the mixture while being added drop-by-drop. When the dispersion was continuously stirred for 30 minutes, the dispersion became black due to H₂ liberation. NaBH₄ was used to reduce GO to rGO and simultaneously to reduce Ferric ion to Fe nanoparticles. So iron oxide in rGO (FGOC) nanocomposite of mass ratio (Fe/GO=1:1) was formed.

2.3 Characterization

The phase analysis study of composite system was executed using CD 100 41 XRD Rigaku unit with a target of copper of 15.4 nm wavelength. For further phase verification, RAMAN spectroscopy was

Table 1 — Description of the adsorbate used in this study

Adsorbate	Methyl Blue
Chemical formula	C ₂₆ H ₂₅ N ₅ O ₁₉ S ₆ Na ₄
Chemical Structure	
Colour Index (C. I.) No.	42780
Colour Index (C. I.) name	Acid blue 22
Molar mass	799.814 g/mol

performed (iHR 500, HORIBA Scientific model). Organic dye removal study was performed by UV-Vis Spectrophotometer (Model Perkin-Elmer Lambda 35).

3 Results and Discussion

3.1.1 X-ray Diffraction Analysis of the Nanocomposites

The X-ray diffraction (XRD) patterns of Graphite, GO, rGO and FGOC nanocomposites are shown in Fig. 1. The most prominent and unique peak of Graphite observed around $2\theta = 26.45^\circ$ corresponding to plane (002) and a small peak around $2\theta = 54.62^\circ$ for (004) plane, are noticed. For GO observed peak around $2\theta = 10.14^\circ$ corresponds (001) plane of diffraction²⁶. Ultrasonication reduces the oxygen-containing functionalities in GO, and this peak disappears. A peak at 2θ value at 26.45° appears as a result, and this is defined as corresponding to (002) plane²⁷. Diffraction peaks at $2\theta = 13.96^\circ, 21.28^\circ, 27^\circ, 36.34^\circ, 46.58^\circ, 49^\circ, 52.68^\circ, 60.28^\circ$ were observed for FGOC corresponding diffraction planes (100), (012), (002), (400) and (440), consistent with rGO and cubic phases of magnetite¹⁹. Based on (002) diffraction plane²⁸, rGO started to form. In addition, (100), (012), (311), (400), (422) and (440) ensured the development of magnetite phase in a composite system.

3.1.2 Fourier Transform Infrared Spectroscopy of the Nanocomposites

Fig. 2 shows the FT-IR spectra of the GO, rGO, Graphite and FGOC samples. There is a

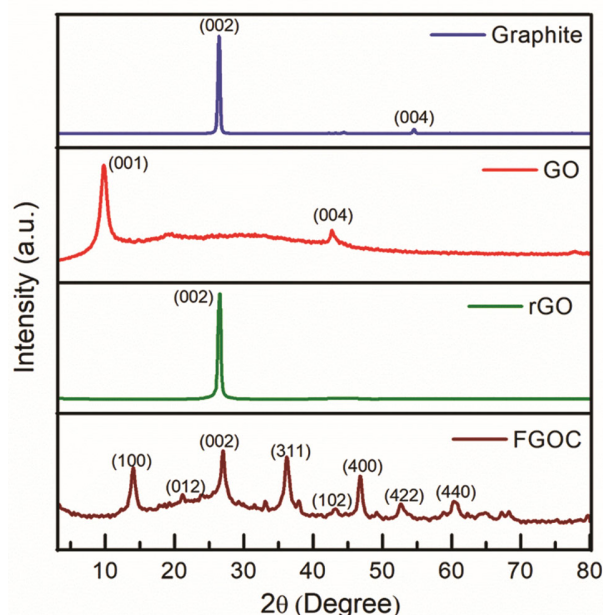


Fig. 1 — XRD patterns of (a) Graphite (b) GO (c) rGO (d) FGOC nanocomposites.

broad absorption band in the GO spectrum at about $3300\text{--}3500\text{ cm}^{-1}$ which is attributed to the stretching vibration from hydroxyl groups in the GO and water absorbed on the GO sheet, and an absorption band at 1730 cm^{-1} ¹⁸. In Fig. 2, some peaks locate at about 3410 cm^{-1} (stretching vibration of -OH), 2920 cm^{-1} (stretching vibration of C-C), 1730 cm^{-1} (stretching vibration of C=O of -COOH), 1620 cm^{-1} (stretching vibration of C=C), 1220 cm^{-1} (tensile vibration of C-N) and 1110 cm^{-1} (asymmetry stretching vibration of C-O-C) of the wavenumber^{29,30}. Compared with Graphite and rGO, the GO has a large number of -OH, -COOH and C-O-C functional groups on its surface that make it hydrophilic. The absorption peak at 1750 cm^{-1} in the spectrum of hydrothermally treated GO almost disappears when NaBH_4 is added during the preparation of FGOC. This could be explained by the reduction of GO's oxygen-containing functional groups during this treatment.

3.1.3 Raman Spectroscopy Studies of the Nanocomposite

In carbonaceous materials, Raman spectroscopy is an important technique for analyzing their underlying properties (like structural). Fig. 3 depicts the Raman spectra for GO, rGO, FGOC nanocomposites inside the wavenumber ranging from 80 cm^{-1} to 2000 cm^{-1} . For the Raman spectrum of GO two important bands D and G bands (Fig. 3) are noticed cresting at 1340 cm^{-1} and 1575 cm^{-1} , respectively^{25,31}. There are two possible explanations for the D band response:

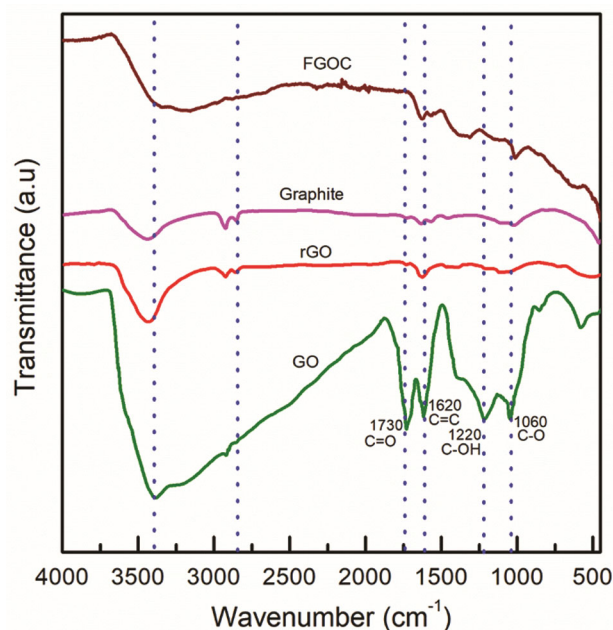


Fig. 2 — FT-IR spectra of (a) GO (b) rGO (c) Graphite (d) FGOC nanocomposites.

either a defect or a breakdown of translational symmetry, and the G band is contrasted by the first-order scattering of the E_{2g} vibration mode generated by the in-plane vibration of sp^2 carbon atoms^{18,32}. Furthermore, the D band intensity differs unambiguously from the G band intensity, based on the disorder degree of the graphic materials^{25,33}. As a result of the breathing mode of A_{1g} symmetry k-phonons, which is observed at higher wavelengths, D-peaks are found at the edges or as defects in graphic structures, since activation of this breathing mode depends on the defects³⁴. The G peak, observed at the lower wavelength, occurs due to the first-order dispersion of doubly degenerate phonons (E_{2g}) in sp^2 order dispersion of doubly degenerated phonons (E_{2g} symmetry) and in sp^2 carbon atoms at the middle of the Brillouin zone²⁵. In Fig. 3, a Raman spectrum showing distinct peaks at approximately 210, 272, 373, 575, 1340, 1575 cm^{-1} can be used to confirm FGOC nanocomposite formation. Carbon atoms in hexangular structure occupy the D band (1332 cm^{-1}), corresponding to a respiration mode. It is in this D band that structural defects develop. Carbon atoms in sp^2 aromatic rings can also be calculated from the vibration of the G band (1567 cm^{-1})¹⁹. As can be seen, the intensity of the D band is higher than the intensity of the G band, which indicates appropriate exfoliation. Intensity magnitude relationships (I_D/I_G) between several D and G bands can be used to

calculate average sp^2 and degree of disorder for several D and G bands. The determined I_D/I_G for GO, rGO and FGOC are 1.02, 1.04 and 1.15 respectively. The determined higher value of I_D/I_G for FGOC indicates that disorder is accumulating when iron nanoparticles are immobilized on GO lattice³⁵. Once the domain size of sp^2 carbon atoms is reduced, the defects which form at the surface edges and ripples lead to better defragmentation³⁶. The higher I_D/I_G value obtained for the FGOC nanocomposite sample confirms the presence of more defects and imperfections than those seen in GO and rGO. A_{1g} , E_g , E_g and E_g vibration modes of Iron Oxide^{19,37} are assigned to peaks around 210 cm^{-1} , 272 cm^{-1} , 373 cm^{-1} and 575 cm^{-1} . It is possible that the dissimilarities are due to the differences in oxygen content or the degree in exfoliation and crystalline size (L_a) between the samples. Analyzing the crystalline size (L_a) of the nanocomposite samples of GO, rGO and FGOC, average carbon atom size is determined. Using Tuinstra-Koenig's relationship³⁸, we determined crystalline size (L_a) of nanocomposite electrolyte membrane type layer structures²⁵

$$L_a (nm) = (2.4 \times 10^{-10}) \times \lambda^4 \times \left(\frac{I_D}{I_G} \right)^{-1} \quad \dots (1)$$

where λ = Laser line wavelength, I_D and I_G represents the Raman peak intensities respectively for the D and the G bands. We observed a significant change in the L_a values as determined 18.85 nm, 18.49 nm and 16.72 nm for GO, rGO and FGOC nanocomposites respectively.

3.2 Effect of Solution pH

The Fig. 4 shows the effect of solution pH onto the FGOC nanocomposites. From this Fig. 4 it is observed that with increasing pH dye adsorption capacity increases. The maximum dye adsorption is observed at pH 7 and thereafter it decreases. The fact can be explained in the following way: at lower pH value the adsorbent surface charge becomes positively charged and also dye molecule gets protonated to $=N^{+/-}$. As a result, electrostatic repulsion occurs between the positively charged surface of the dye molecule and the positively charged surface of the adsorbent reducing adsorption capacity. As solution pH increases the dye molecule gets negatively charged due to the deprotonation of sulfonic acid

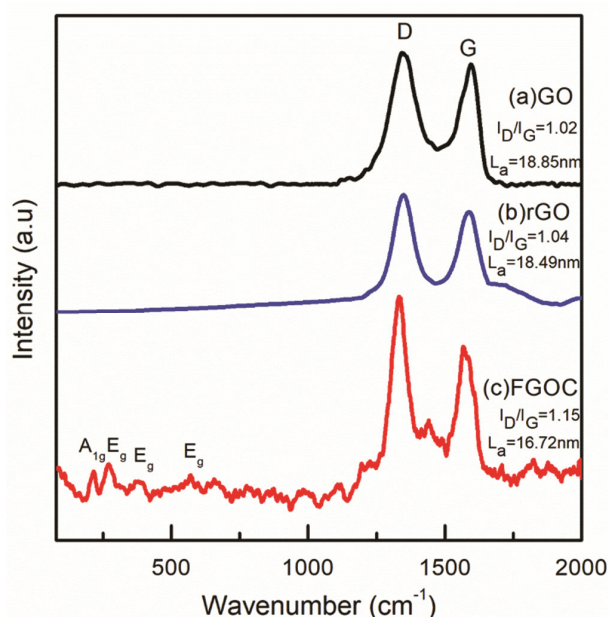


Fig. 3 — Raman spectra of (a) GO (b) rGO (c) Graphite (d) FGOC nanocomposites.

group to sulfonate which enhancing electrostatic attraction between the positively charged FGOC and negatively charged sulfonate resulting an increase the dye adsorption capacity. Similar results agree well with previous reports³⁹.

3.3 Effect of Initial Methyl Blue Concentration on Adsorption

For dye removal the fact that, GO is an effective adsorbent for cationic dyes like Methylene Blue while rGO is an effective adsorbent for anionic dyes¹. Our composite contains rGO so it behaves accordingly. We find that Methylene Blue is not at all adsorbed by the composite. Guo *et al.*¹⁸ studied the adsorption of Methyl Blue (which is different from Methylene Blue) and obtained rapid and high adsorption. We also studied Methyl Blue by our composite. In a composite, the increase of adsorption sites and enhancement of interaction of dye molecules are the main causes of the rapid and efficient removal of dyes. Guo *et al.*¹⁸ had remarked rapid decolouration of Methyl Blue is due to the increase of adsorption site. This following equation¹⁸ was used to determine Methyl Blue adsorption capacity per unit mass of adsorbent:

$$q = \frac{(C_0 - C_t)V}{C_0} \quad \dots (2)$$

where, q is the adsorption capacity of adsorbent (mg/g); C_0 and C_t are the Methyl Blue concentration

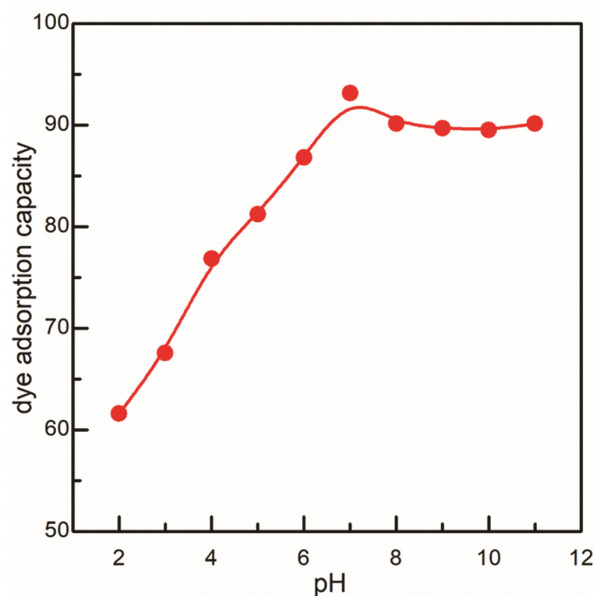


Fig. 4 — Variation of pH onto the percentage of dye removal from Methyl Blue aqueous solution of different pH by FGOC nanocomposite.

(mg/L) before and after adsorption for a certain time, respectively; t is the adsorption time (min); m is the adsorbent mass (g); V is the initial volume of Methyl Blue solution (L).

Fig. 5 shows the effect of the initial Methyl Blue concentration on the absorption performance of FGOC under the chosen condition (100 mL of Methyl Blue solution, 1 g/L of adsorbent dosage, 7 of pH value, and 40 °C of adsorption temperature). At the initial stage, the adsorption rate is fast due to a large number of adsorption vacancies on the adsorbent. This is a time-dependent stage. At the second stage, the adsorption rate is relatively slow, and concentration is the most influential factor. When the concentration of Methyl Blue is increased, its adsorption capacity will increase as well. This is because it is difficult for the remaining vacant active sites to be occupied at this stage. The higher the concentration of Methyl Blue per unit volume, the greater the probability of being captured by FGOC NPs, and the stronger the adsorption capacity.

3.4 Kinetics of adsorption

In order to understand the Methyl Blue adsorption mechanism on FGOC nanocomposite, the Methyl Blue adsorption kinetics were studied by using the quasi-first-order and quasi-second-order kinetic models. The corresponding equations are as follows³⁹:

$$\text{Quasi-first-order model: } \ln(q_e - q_t) = \ln q_e - \frac{k_1 t}{2.303} \quad \dots (3)$$

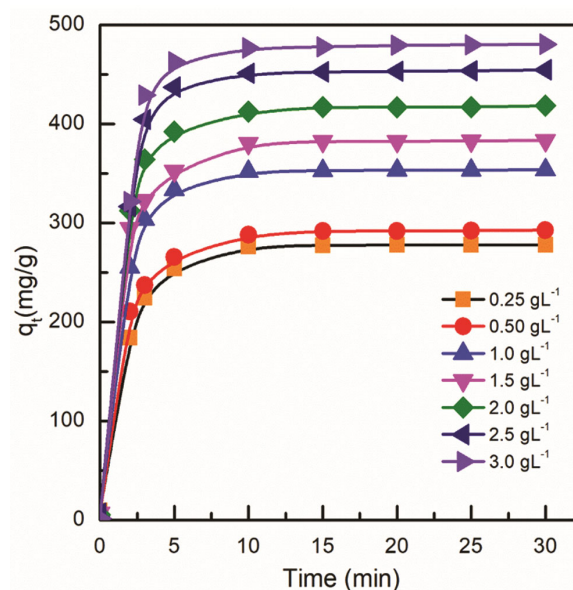


Fig. 5 — Variations of the adsorption capacity (q_t) of FGOC with time for different Methyl Blue concentrations.

$$\text{Quasi-second-order model: } \frac{t}{q_t} = \frac{1}{k_2 q_e^2} + \frac{t}{q_e} \quad \dots (4)$$

where, q_e and q_t are the amounts of Methyl Blue adsorbed (mg/g) at equilibrium and at a certain adsorption time, t is the adsorption time (min), k_1 (min^{-1}) and k_2 ($\text{g/mg}\cdot\text{min}$) are the quasi-first and quasi-second orders rate constants, respectively. Table 2 summarizes the kinetic constants obtained by linear regression for the two models (Fig. 6).

The fitted linear correlation of the quasi-second-order kinetic equation is much higher than that of the quasi-first-order kinetic equation, and the theoretical maximum adsorption capacity calculated by the quasi-second-order kinetic equation has little difference with the experimental value. In other words, the Methyl Blue adsorption on FGOC is more consistent with the quasi-second-order kinetic model, indicating the chemisorption characteristic. The reason may be that the abundant oxygen-containing functional groups in GO provide lone pair electrons to form a complex with Methyl Blue on the adsorbent.

3.5 Adsorption isotherm

In order to reveal further the Methyl Blue adsorption mechanism of FGOC, Langmuir⁴⁰ & Freundlich⁴¹ models are used to fit the adsorption isotherm. Isotherm studies can describe the interaction between adsorbate and adsorbent and provide the most important parameters for designing ideal adsorption system. Langmuir adsorption-isotherm model assumes monolayer surface adsorption. The solid surface is uniform and there is no interaction between the adsorbed molecules. On the contrary, Freundlich adsorption-isotherm model assumes heterogeneity of adsorption surfaces. Equation (5) and (6) are their corresponding adsorption equations, respectively

$$\text{Langmuir isotherm: } \frac{c_e}{q_e} = \frac{c_e}{q_{\max}} + \frac{1}{k_L q_{\max}} \quad \dots (5)$$

$$\text{Freundlich isotherm: } \log q_e = \log k_f + \frac{1}{n} \log c_e \quad \dots (6)$$

where c_e and q_e are adsorption concentration (mg/g) and equilibrium adsorption capacity (mg/g), q_{\max} is the Langmuir monolayer adsorption capacity (mg/g),

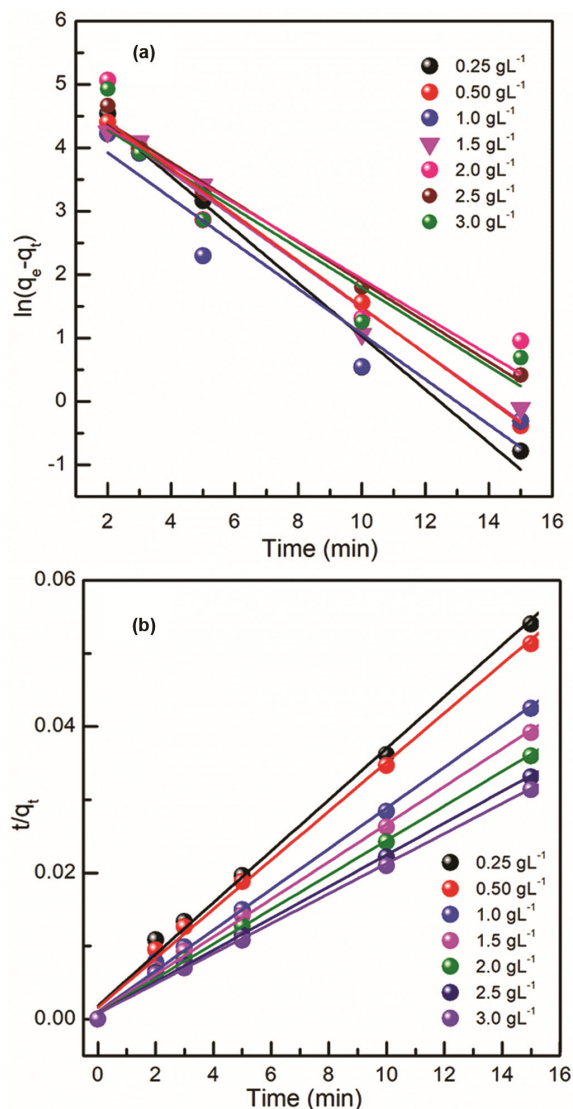


Fig. 6 — Quasi-first-order kinetics (a) and Quasi-second-order kinetic (b) of MB adsorption on the FGOC nanocomposite.

Table 2 — Adsorption kinetic parameters of Methyl Blue by FGOC nanocomposite.

C_0 [g/L]	Quasi-first-order kinetics				Quasi-second-order kinetics		
	k_1 [min^{-1}]	$q_{e,\text{cal}}$ [mg/g]	$q_{e,\text{exp}}$ [mg/g]	R^2	k_2 [g/mg/min]	$q_{e,\text{cal}}$ [mg/g]	R^2
0.25	0.9678	279.78	278.13	0.97835	0.0067	284.09	0.9996
0.5	0.8867	139.40	292.83	0.98828	0.0068	298.51	0.9994
1.0	0.8843	102.84	353.81	0.99184	0.0073	358.42	0.9995
1.5	0.8232	174.75	383.48	0.97731	0.0067	389.11	0.9996
2.0	0.7872	121.65	418.58	0.90345	0.0065	423.73	0.9996
2.5	0.7172	95.18	454.78	0.98514	0.0061	460.83	0.9994
3.0	0.7164	84.01	480.55	0.87802	0.0053	487.81	0.9992

Table 3 — The parameters of Langmuir and Freundlich adsorption Isotherms models of Methyl Blue adsorbed by FGOC nanocomposite.

Langmuir adsorption Isotherms			Freundlich adsorption Isotherms			
$q_{\max}(\text{mg/g})$	$k_L(\text{L/mg})$	R^2	R_L	$k_F(\text{L/mg})$	n	R^2
480.55	0.0026	0.9931	1.53846 - 0.12821	6.52	4.394	0.9594

k_L and k_F are the Langmuir and Freundlich constants (L/mg) respectively, and n is the Freundlich constant associated to adsorption intensity.

Using a dimensionless equilibrium parameter R_L^{42} , we can define the Langmuir isotherm as follows:

$$R_L = \frac{1}{1 + k_L C_0} \quad \dots (7)$$

If C_0 , the initial concentration of MB (mg/L), the R_L value indicates whether Langmuir isotherm is favorable ($0 < R_L < 1$), unfavorable ($R_L > 1$), linear ($R_L = 1$) and irreversible ($R_L = 0$). From Fig. 7(a) we get the value of R_L 1.53846, 0.76923, 0.38462, 0.25641, 0.19231, 0.15385, 0.12821 for C_0 250, 500, 1000, 1500, 2000, 2500 and 3000mg/L respectively. We see that for initial concentration of MB 500-3000 mg/L the value of R_L is favorable. Fig. 7 shows the equilibrium isotherms for the Methyl Blue adsorption on the FGOC nanocomposite. The linear correlation coefficient R^2 values obtained from Langmuir and Freundlich linear equations are 0.9931 and 0.9594, respectively. The parameters of Langmuir and Freundlich adsorption Isotherms models of Methyl Blue adsorbed by FGOC nanocomposite are shown in Table 3. It could be seen that the correlation coefficient fitted by Langmuir model is much higher than that of Freundlich model, and the theoretical saturated adsorption capacity of 500 mg/g is very close to the experimental value of 480.55 mg/g. This indicates that monolayer adsorption and non-uniform surface adsorption exist simultaneously, but monolayer chemisorption plays a dominant role in the adsorption process^{43,44}.

4 Conclusions

The FGOC nanocomposites were successfully prepared by solution mixing technique and applied for methyl blue removal in wastewater. Following an adsorption regeneration strategy, the majority of industrial gas and liquid operations are carried out in adsorbent-based fixed beds. In a fixed bed, adsorption is frequently used to remove a solute from a liquid solution. Several factors influence the adsorption rate in a bed or a portion of one. Solute diffusion through

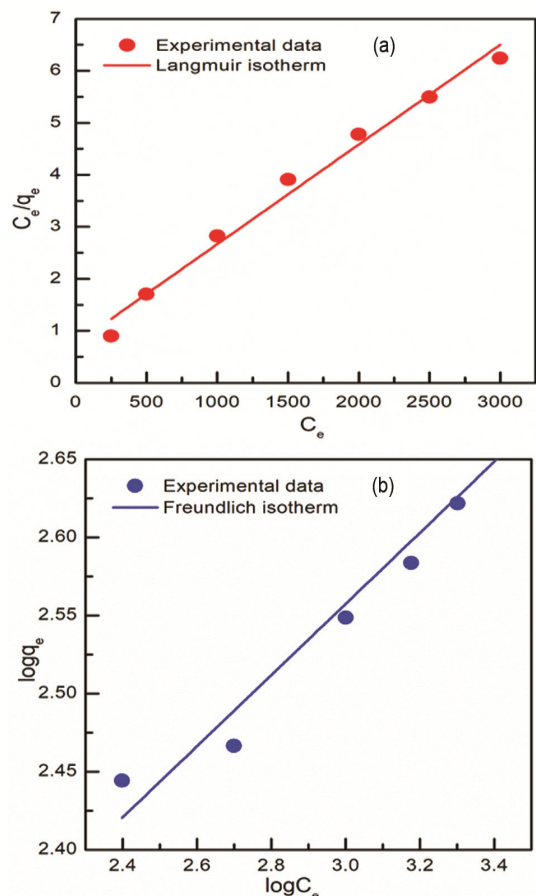


Fig. 7 — (a) Langmuir adsorption Isotherms (b) Freundlich adsorption Isotherms for Methyl Blue on FGOC nanocomposite.

the adsorbent particle pores (macro, meso and micro pores) causes two-mass transfer resistances in series: (i) the resistance to the transport of the solute through a stagnant gas film to the particle's surface, and (ii) that due to diffusion through the pores of the particle to reach the adsorption site within the particle. Adsorption kinetic resistance may potentially be a result of the adsorption of solute molecules at the active sites. When the intrinsic adsorption rate is high, it is possible to ignore the resistance. Thus, the concentration gradient of the solute in a particle is frequently seen. The negative charge of Methyl Blue ($-\text{SO}_3^-$) decreases the dye's adsorption capacity because it makes it repellant to GO surfaces. However, the negatively charged parts of the dye

molecules ($-\text{SO}_3^-$) are more easily absorbed by the positively charged H^+ ions present on the rGO as well as FGOC nanosheets. The ion effect is more pronounced when Methyl Blue dye molecules bind to rGO nanosheets than when they bind to GO nanosheets. As our sample FGOC nanocomposite contains rGO with iron oxide, here we used MB, dye is used. An external magnet can also be used to separate the composite after dye adsorption from the treated wastewater since it is magnetic. The MB adsorption on the FGOC composite is dominated by chemisorption. The results clearly demonstrate that this kind of FGOC nanocomposite has great potential as an adsorbent for Methyl Blue removal from wastewater.

Acknowledgements

The work is carried out with the financial support from RUSA 2.0 component: 8 to Midnapore College (Autonomous), India and also with the needful assistances from the Department of Chemistry of Vidyasagar University and CRF, IIT Kharagpur, India.

References

- Ramesha G K, Kumara A V, Muralidhara H B & *J Colloid Interface Sci*, 361 (2011) 270.
- Yang S T, Chen S, Chang Y, Cao A, Liu Y & Wang H, *J Colloid Interface Sci*, 359 (2011) 24.
- Zhang W, Zhou C, Zhou W, *et al.*, *Bull Environ Contam Toxicol*, 87 (2011) 86.
- Liu F, Chung S, Oh G & Seo T S, *ACS Appl Mater Interfaces*, 4 (2011) 922.
- Liu T, Li Y, Du Q, Sun J, Jiao Y, Yang G, Xia Y, Zhang W, Wang K, Zhu H & Wu D, *Biointerfaces*, 90 (2012) 197.
- Li Y, Du Q, Liu T, Peng X, Wang J, Sun J, Wang Y, Wu S, Wang Z, Xia Y & Xia L, *Chem Eng Res Des*, 91 (2013) 361.
- Yang X, Li Y, Yanhui, Du Q, Wang X, Hu S, Chen L, Wang Z, Xia Y & Xia L, *J Nanosci Nanotechnol*, 16 (2016) 1775.
- Heidarizad M & Şengör S S, *J Mol Liq*, 224(A) (2016) 607.
- Akbar F, Kolahdouz M, Larimian S, Radfar B & Radamson H H, *J Mater Sci: Mater Electron*, 26 (2015) 4347.
- Cao J, Liu Q, Du J, Yang L, Wei M, Gao M & Yang J, *J Mater Sci: Mater Electron*, 28 (2017) 2267.
- Peng Q Q, Liu Y G, Zeng G M, Xu W H, Yang C P & Zhang J J, *J Hazard Mater*, 177 (2010) 676.
- Huang T, Dai J, Yang J H, Zhang N, Wang Y & Zhou Z W, *Diam Relat Mater*, 86 (2018) 117.
- Jaleh B, Khalilipour A, Habibi S, Niyafar M & Nasrollahzadeh M, *J Mater Sci: Mater Electron*, 28 (2017) 4974.
- Ranjith R, Ravikumar S, Pandiyan V, Rajaji U, Abualnaja K M, AlMasoud A T S & Ouladsmne M, *J Mater Sci: Mater Electron*, 33 (2022) 9438.
- Huong P T L, Son T V, Pham V N, Tam L T & Le A T, *J Nanosci Nanotechnol*, 18 (2018) 5591.
- Liu M C, Wen T, Chen C L, Hu J, Li J & Wang X K, *Dalton Trans*, 42 (2013) 14710.
- Jinendra U, Bilehal D, Nagabhushana B M, Kumara K S J & Kollur S P, *Heliyon*, 7 (2021) 6070.
- Guo J, Wang R, Tjiu W W, Pan J & Liu T, *J Hazard Mater*, 63 (2012) 225.
- Pradhan S S, Konwar K, Ghosh T N, Mondal B, Sarkar S K & Deb P, *Colloid Interface Sci Commun*, 39 (2020) 100319.
- Zhou C, Zhang W, Wang H, Li H, Zhou J, Wang S, Liu J, Luo J, Zou B & Zhou J, *Arab J Sci Eng*, 39 (2014) 6679.
- Huong P T L, Huyen N T, Giang C D, Tu N, Phan V N, Quy N V, Huy T Q, Hue D T M, Chinh H D & Le A T, *J Nanosci Nanotechnol*, 16 (2016) 9544.
- Chong S, Zhang G, Tian H & Zhao H, *J Environ Sci*, 44 (2016) 148.
- El-Shafai N M, El-Khouly M E, El-Kemary M, Ramadan M S & Masoud M S, *RSC Adv*, 8 (2018) 13323.
- Hummers W S & Offeman R E, *J Am Chem Soc*, 80 (1958) 1339.
- Ghosh T N, Pradhan S S, Sarkar S K & Bhunia A K, *J Mater Sci: Mater Electron*, 32 (2021) 19157.
- Bahrami A, Kazeminezhad I & Abdi Y, 125 (2019) 125.
- Zhang J, Yang H, Shen G, Cheng P, Zhang J & Guo S, *Chem Commun*, 46 (2010) 1112.
- Kumar S, Chinnathambi S, Scanlon L G & Munichandraiah N, *Phys Chem Chem Phys*, 16 (2014) 22830.
- Zhu X, Zhu Y, Murali S, Stoller M D & Ruoff R S, *ACS Nanomater*, 5 (2011) 3333.
- Zhang G K, Gao Y Y, Zhang Y L & Guo Y D, *Environ Sci Technol*, 44 (2010) 6384.
- Muzyka R, Drewniak S, Pustelny T, Gryglewicz G & Smezdowski Ł, *11th Conf Integr Opt: Sens, Sens Struct Meth*, 100340C (2016).
- Fang M, Wang K, Lu H, Yang Y & Nutt S, *J Mater Chem*, 20 (2010) 1982.
- Wang Y Y, Ni Z H, Yu T, Shen Z X & Wang H M, *J Phys Chem C*, 112 (2008) 10637.
- Stankovich S, Dikin D A, Piner R D, Kohlhaas K A, Kleinhammes A, Jia Y, Wu Y, Nguyen S T & Ruoff R S, *Carbon*, 45 (2007) 1558.
- Xing M & Wang J, *J Colloid Interf Sci*, 474 (2016) 119.
- El-Shafai N M, El-Khouly M E, El-Kemary M, Ramadan M S & Masoud M S, *RSC Adv*, 8 (2018) 13323.
- Saikia K, Bhattacharya K, Sen D, Kaushik S D, Biswas J, Lodha S, Gogoi B, Buragohain A K, Kockenberger W & Deb P, *Appl Surf Sci*, 464 (2019) 567.
- Cancado L, Takai K & Enoki T, *Appl Phys Lett*, 88 (2006) 163106.
- Sharma P, Hussain N, Borah D J & Das M R, *J Chem Eng Data*, 58 (2013) 3477.
- Langmuir I, *J Am Chem Soc*, 40 (1918) 1361.
- Freundlich H M F, *Z Phys Chem*, 57 (1906) 385.
- Weber T W & Chakravorti R K, *J Am Inst Chem Eng*, 20 (1974) 228.
- Ai L H, Zhang C Y & Chen Z L, *J Hazard Mater*, 192 (2011) 1515.
- Lin Y F, Chen H W, Lin K L, Chen B Y & Chiou C, *J Environ Sci*, 23 (2011) 44.